








Paleoglacial footprint and fluvial terraces of the Shaluli Shan, SE Tibetan Plateau

R. A. A. Schneider ^{a,b}, R. Blomdin ^c, P. Fu ^d, X.K. Xu ^{e,f} and A. P. Stroeven ^{a,b}

^aGeomorphology and Glaciology, Department of Physical Geography, Stockholm University, Stockholm, Sweden; ^bBolin Centre for Climate Research, Stockholm University, Stockholm, Sweden; ^cGeological Survey of Sweden, Uppsala, Sweden; ^dDepartment of Geographical Sciences, University of Nottingham Ningbo China, Ningbo, People's Republic of China; ^eInstitute of Tibetan Plateau Research and Center for Excellence in Tibetan Plateau Earth Sciences, Chinese Academy of Sciences, Beijing, People's Republic of China; ^fKey Laboratory of Tibetan Environment Changes and Land Surface Processes, Institute of Tibetan Plateau Research, CAS, Beijing, People's Republic of China

ABSTRACT

This study provides mapping of glacial and fluvial geomorphology in the Shaluli Shan region on the eastern margin of the south-eastern Tibetan Plateau. Based on TanDEM-X 12 m elevation data and GoogleEarth imagery, glacial valleys, ice-marginal moraines, glacial lineations, scoured terrain and fluvial terraces were mapped. Covering around 11,000 km², this map is the first for this region to display geomorphology at a spatial resolution of 0.4 arcsec (= c. 11 m) and to include fluvial terraces. Its glacial landform distribution is largely consistent with previous mapping. The substantially higher level of detail in this study is reflected in an approximately tenfold number and smaller median sizes of individual landforms such as moraines and glacial lineations. These results underscore the importance of high-resolution DEM data such as TanDEM-X for the identification of glacial and fluvial geomorphology. The map presented here will be used for detailed paleoglacial reconstructions and landscape evolution studies combining both glacial and fluvial landforms.

ARTICLE HISTORY

Received 14 January 2021
Revised 31 May 2021
Accepted 15 June 2021

KEYWORDS

TanDEM-X; SE Tibetan Plateau; paleoglaciology; fluvial terrace; ice-marginal moraine; glacial valley

1. Introduction


Global climate change induces an increasing need to understand spatial, temporal, and ultimately causal relationships between climate and landscape development. Moreover, landscapes are sensitive to changes in exogenic (climatic) and endogenic (tectonic) forcing and their responses can be complex (Cordier et al., 2017; Molnar & England, 1990; Raymo & Ruddiman, 1992). This complexity typically results in palimpsest landform assemblages formed by one process coexisting with, or overprinted by, a landform assemblage of another process (Glasser & Bennett, 2004; Schmidt & Andrew, 2005).

Due to its dimension (Figure 1), the Tibetan Plateau exerts a regional dominance on atmospheric circulation patterns (Yao et al., 2013; Zhang et al., 2018), reflected in the extents of glaciers and their trajectories of change (Yao et al., 2012a). This is because glacier mass balance, and ultimately glacier extent, is highly sensitive to temperature and precipitation (Oerlemans & Fortuin, 1992). Reconstructions of glacier extent can therefore serve as evaluation datasets for glacier and climate modelling (Owen & Dortch, 2014; Yan et al., 2018). Evaluating climate proxy data (e.g. Liu et al., 2020; Yao et al., 2007) against paleoglacial

reconstructions can reveal if glaciation on the Tibetan Plateau is most sensitive to changes in precipitation or temperature (e.g. Dortch et al., 2013). Nonetheless, these relationships remain challenging to disentangle, in part because of tectonic activity. Uplift affects climate and drives or modifies responses in glaciation on geological timescales and adds an additional layer of complexity to landscape evolution reconstructions (Owen & Dortch, 2014).

To add further complexity, strong regional gradients in the response of glaciers to increases in temperature and concomitant changes in precipitation have been observed on the Tibetan Plateau (Farinotti et al., 2020; Hewitt, 2005; Yao et al., 2012a). Controversies about the timing and extent of past glaciations remain. Spatial gradients in the timing and extent of paleoglaciation have been inferred between the southern and eastern margins of the Tibetan Plateau, which receive snowfall from monsoon circulation, and its western and northern margins that are dominated by snowfall supplied by westerly circulation (Lehmkuhl & Owen, 2005; Owen & Dortch, 2014; Yan et al., 2020). This diverse evidence indicates that glaciers on the Tibetan Plateau respond, and have responded, to climate change in complex ways. This

CONTACT R.A.A. Schneider  ramona.schneider93@web.de

 Supplemental data for this article can be accessed at <https://doi.org/10.1080/17445647.2021.1946443>.

© 2021 The Author(s). Published by Informa UK Limited, trading as Taylor & Francis Group.

This is an Open Access article distributed under the terms of the Creative Commons Attribution License (<http://creativecommons.org/licenses/by/4.0/>), which permits unrestricted use, distribution, and reproduction in any medium, provided the original work is properly cited.

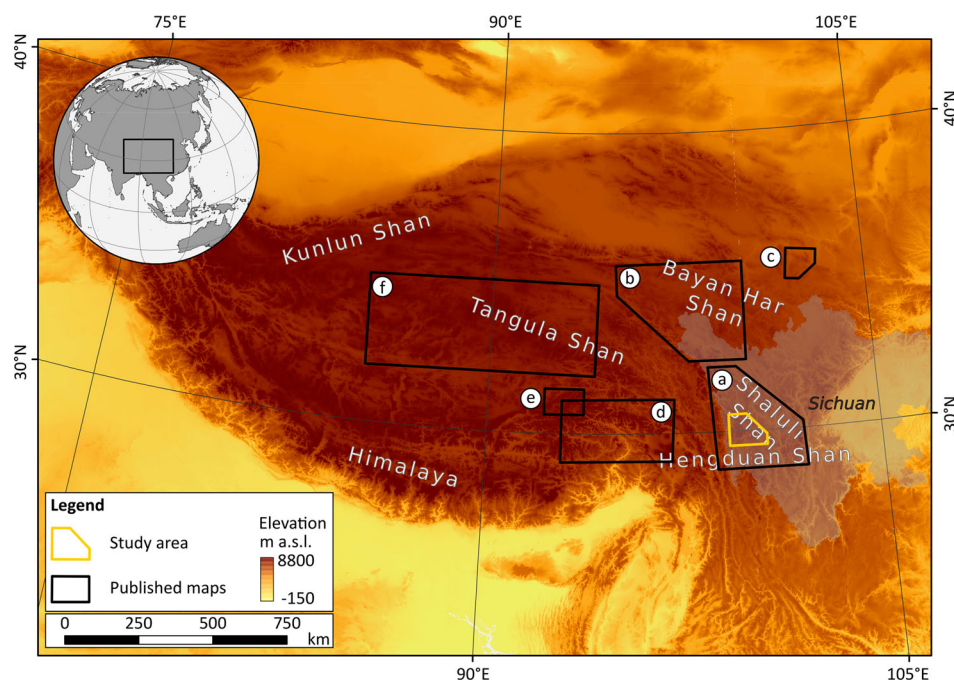


Figure 1. The Tibetan Plateau and location of the study area (yellow polygon; Figure 2) and previously published glacial geomorphological maps (black polygons). (a) Shaluli Shan (Fu et al., 2012); (b) Bayan Har Shan (Heyman et al., 2008); (c) Dalijia Shan (Kassab et al., 2013); (d) Parlung Zangbo Valley, (Chen et al., 2016); (e) Maidika region (Lindholm & Heyman, 2016); (f) Tangula Shan (Morén et al., 2011). Overview map of the Tibetan Plateau, indicating the mapping area of this and of previous mapping studies.

may partly reflect tectonic modification of the glacier response to climate change (Barr & Lovell, 2014; Shulmeister et al., 2009). Consequently, the question to which degree temperature decreases or precipitation increases drive Tibetan Plateau glacial advances remains unresolved (Chevalier & Replumaz, 2019; Murari et al., 2014; Owen & Dortch, 2014).

It is conceivable that some of the spatial and temporal complexity derives from a lack of detailed geomorphological mapping and associated dating of glacial landforms (Fu et al., 2013a, 2013b; Heyman et al., 2008; Owen & Dortch, 2014). While such mapping is essential for accurate, detailed, and meaningful reconstruction of paleoenvironments, in practice it is often limited by the availability of high-resolution data and imagery. Previous geomorphological mapping of the Tibetan Plateau and surrounding mountain ranges has primarily been based on digital elevation models with spatial resolutions of 30–90 m (e.g. SRTM and ASTER), Landsat ETM+ satellite imagery (30 m horizontal resolution, 15 m for its panchromatic band), and, in some studies, Google Earth imagery (Figure 1).

This paper advances previous mapping of the Shaluli Shan region on the south-eastern margin of the Tibetan Plateau in two critical aspects and ultimately contributes to a reconstruction of its paleoglacial history and landscape evolution. First, we utilise high-resolution TanDEM-X 12 m data to map glacial landforms (glacial valleys, ice-scoured terrain, ice-marginal moraines, and glacial lineations) in

unprecedented detail. There are individual studies that utilise TanDEM-X data for geomorphological purposes (e.g. Boulton & Stokes, 2018; Grohmann, 2018; Pasquetti et al., 2019; Pánek et al., 2020; Pipaud et al., 2015; Viveen et al., 2020), but to our knowledge, this is the first study employing such high-resolution data for the purpose of extensive geomorphological mapping on the Tibetan Plateau. A geomorphological map of glacial landforms in the Shaluli Shan region was presented by Fu et al. (2012). However, because they used SRTM and Landsat ETM+, the availability of 12 m TanDEM-X in this study enables a considerable increase in the level of detail at which landforms are mapped.

Geomorphological mapping for paleoglacial research commonly focusses on glacial landforms (e.g. Glasser & Bennett, 2004). To add a systematic mapping of fluvial terraces to glacial features is novel for this region. It also is the prime reason for employing TanDEM-X data because it provides the required spatial resolution, as shown by the mapping of fluvial terraces elsewhere (Charrier & Li, 2012; Viveen et al., 2020). We here jointly map glacial and fluvial landforms as part of one study to distinguish between climatic and tectonic drivers of landscape evolution. This is because river terrace sequences form through cycles of sediment deposition and fluvial incision and their formation has been mainly attributed to climatic cyclicity, even though tectonic uplift also favours their formation (e.g. Bridgland & Westaway, 2008; Maddy et al., 2001; Olszak, 2017; Starkel, 2003).

The purpose of this study is to test and illustrate the potential of 12 m TanDEM-X for high-resolution mapping of glacial and fluvial landforms. As an added advantage, it also provides a comparison dataset to the mapping of glacial landforms conducted by, and the reconstruction of the glacial footprint presented in Fu et al. (2012). The resulting main map has guided the identification of targets for geochronological research and field studies in support of paleoglacial and landscape evolution studies on a regional scale.

2. Study area and previous research

The Tibetan Plateau is a unique topographic feature with an average elevation of more than 4000 metres above sea level and an extent of 5 million km² (Fielding et al., 1994; Yao et al., 2012b). It started uplifting during the early Cenozoic as the Central Asian and Indian plates collided, with profound consequences for landscape evolution and global and regional climate change (Clark et al., 2005; Raymo & Ruddiman, 1992; Wang et al., 2008, 2012; Yao et al., 2012b). Because of its importance for climate dynamics, considerable efforts have been made to reconstruct climate change from the history of glaciation on the Tibetan Plateau and surrounding mountain ranges through glacial geomorphological mapping and geochronological studies (Blomdin et al., 2016a, 2016b, 2018; Chen et al., 2016; Chevalier & Replumaz, 2019; Gribenski et al., 2018; Heyman et al., 2008, 2009, 2011a, 2011b; Lehmkuhl & Owen, 2005). Most of these recent studies conclude that alpine-style glaciation has dominated on the Tibetan Plateau, with strong regional differences in the timing of maximum glaciation across the region (Blomdin et al., 2016b; Owen & Dortch, 2014).

The Shaluli Shan mountain range extends for 450 km in a north–south direction and is part of the Hengduan Mountains forming the southeastern margin of the Tibetan Plateau (Figures 1 and 2). The study area is located in the province of Sichuan, China, and encompasses around 11,000 km² of the central part of the Shaluli Shan (Figure 1). The regional topography is characterised by high, deeply-incised mountain ranges and low-relief granitic plateaus such as the Haizishan Plateau, which are interpreted to be remnants of an older, uplifted paleosurface (Figure 2; Clark et al., 2005). Past and present-day tectonic activity results from active faults intersecting the Shaluli Shan, for example the Litang fault system (Figure 2), and is expressed in the presence of pull-apart basins, landform displacements, and rockfalls triggered by earthquakes (Chevalier et al., 2016; Zeng et al., 2019).

An abundance of preserved glacial landforms in the Shaluli Shan have attracted research on its regional paleoglacial history (Chevalier & Replumaz, 2019; Fu et al., 2012, 2013a, 2013b, 2019; Xu & Zhou, 2009,

2014; Zhang et al., 2015). Extensive geomorphological mapping of the Haizishan Plateau using SRTM, Landsat ETM+ satellite imagery, and field-based paleogeological observations, revealed zonal patterns of glacial erosion and deposition indicative of a former ice cap (Fu et al., 2012, 2013a) with outlet glaciers descending the plateau flank and, where present, into the pull-apart basins. The presence of a polythermal paleo ice cap on the Haizishan Plateau was further corroborated by cosmogenic nuclide exposure dating and numerical glacier modelling (Fu et al., 2013b, 2019). It is expressed in the landscape as relict and scoured terrains on top of the Haizishan Plateau and linear erosion of glacial valleys on its flanks, defining zones of differing erosion strength.

3. Materials and methods

3.1. Data and map production

Geomorphological mapping of glacial landforms and fluvial terraces was performed using TanDEM-X 12 m digital elevation data. To map glacial landforms, including ice-marginal moraines marking the maximum extent of glaciation (end moraines), in close proximity to fluvial terraces, we chose a map area that covers the Ge'Nyen massif and the northern part of the Haizishan Plateau (the main source areas of the maximum glaciation) and three tectonic basins, which serve as storage areas for fluvial sediments.

Geomorphological mapping relies on the premise that landforms have characteristic appearances which allow them to be delineated and classified (Hubbard & Glasser, 2005; Minár & Evans, 2008). Factors such as the size of the investigation area, age and degradation of targeted landforms, applied mapping methodology, and the purpose of the final map product will determine applied classification criteria. Transparency regarding the mapping criteria and techniques is therefore a fundamental part of mapping ethics (Chandler et al., 2018).

Here, a pre-defined set of criteria guided the mapping from remotely sensed imagery (Table 1) and cross-checking of the mapping was achieved for several key areas during field observations in June 2019 (field verification route shown in black in Figure 2). We used four tiles of 12 m TanDEM-X with a local spatial resolution of 11.11 m (Wessel, 2018) and combined this with Google Earth imagery for perspective viewing where additional clarification was required. Mapping was conducted in ArcMap through manual delineation of landforms and interpretation of TanDEM-X hillshade-derivatives, using different azimuth (315°, 280°, 0°, 45°, 80°) and zenith (10°, 20°) values, which defines the angle of incoming insolation and the pattern of shading. The use of a range of

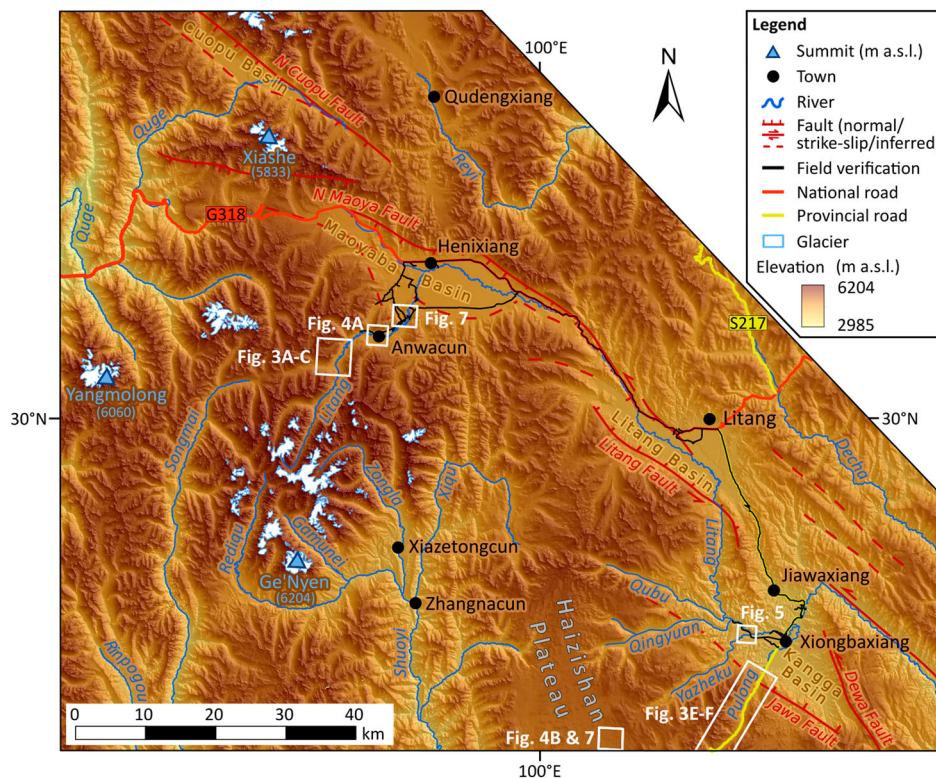


Figure 2. Physiography of the research area. Hillshade of TanDEM-X elevation data illustrates topography (© DLR 2019). Black line shows the field work route along which field verification was performed. Faults comprising the Litang fault system are from Chevalier et al. (2016). White rectangles indicate locations of Figures 3–5 and 7. Glacier data: GLIMS (2018), version 20191217 (<https://www.glims.org/download/>). Map showing the physiography of the research area, including main summits, rivers, towns, major roads, and tectonic faults. Field verification route outlines the areas which were visited in 2019. Background is a TanDEM-X-based hillshade.

illumination angles is important because shadowing affects the level of detail at which landforms can be mapped.

The methodology for mapping of glacial landforms follows the framework for best practice (Chandler et al., 2018) and is comparable with previous mapping strategies on the Tibetan Plateau. Individual landforms were identified and mapped by iterative passes over the mapping area at different scales (for exceptionally large or small landforms, the applied on-screen mapping scales may have varied):

- 1:100,000 – large-scale identification of glacial valleys, large ice-marginal moraines, scoured terrain, and glacial lineations
- 1:50,000 – identification of smaller ice-marginal moraines, mapping of glacial valleys, and glacial lineations
- 1:25,000 – mapping of ice-marginal moraines and glacial valley heads (cirques)
- 1:5000 –1:10,000 – validation and refinement of map details

The distribution of contemporary glaciers comes from the Global Land Ice Measurements from Space glacier database (GLIMS).

3.2. Mapped landforms and identification criteria

Glacial valleys, ice-marginal moraines, scoured terrain, and glacial lineations are mapped because of their paleoglaciological significance (Glasser & Bennett, 2004). In addition to these glacial landforms, fluvial terraces were identified as part of a larger project to understand whether their formation by fluvial deposition and incision is intrinsically coupled to the advance and retreat of glaciers. Identification and detailed mapping of these landforms largely depend on the spatial resolution of available data and hillshade illumination angles. Consistent mapping results require detailed landform identification criteria and recognition of potential error sources. These are adapted for mapping from TanDEM-X from previous studies (Blomdin et al., 2016a; Fu et al., 2012; Heyman et al., 2008; Stroeven et al., 2013) and outlined in Table 1.

Glacial valleys are smooth valleys, sometimes with truncated spurs or lake-filled overdeepenings, and with U-shaped or parabolic cross profiles that, because of their commonly km-scale size, often stand out from remote sensing and topographic data. They form when glaciers deepen and widen pre-existing valleys (Figure 3; Li et al., 2005; Benn & Evans, 2013). Some

Table 1. Identification criteria, typical dimensions, possible identification errors, and geomorphological significance of the landforms mapped in this study.

Landform	Identification criteria	Dimensions	Possible identification errors	Significance	Mapping procedure	Reference
Glacial valley	U-shaped or parabolic cross-profile; often irregular long profiles with alternating flat and steep parts (often due to overdeepened sections). Sometimes associated with hanging valleys. Lack of interlocking spurs which are typical for fluvial valleys.	Several kilometres in width and length	Errors may occur if U-shape is not distinct or obscured by the effects of fluvial or hillslope processes, and sediment infill. Identification of the lowest downvalley extent can be challenging.	Indicative of erosion by valley glaciers, requires multiple glacial cycles	Outlining of valley extents as polygons as identified from slope rasters and hillshades. Profiling tool can be employed to visually determine transitions from upstream parabolic valley-profiles to downstream V-shaped valley-profiles.	Fu et al. (2013a); Blomdin et al. (2016a)
Ice-marginal moraine	Ridge composed of unsorted glaciogenic material. Crest can be linear to sinuous and sharp if ice cored. Forms alongside (lateral moraine) or transverse (terminal moraine) to glacier flow direction	Several hundred metres long, tens to hundreds of metres wide, several to tens of metres high	Delineation of moraine extents can be challenging if till cover is thin or fragmented. Small features close to spatial resolution of the DEM can be difficult / impossible to identify.	Ice-marginal landform, indicative of glacier extent and shape.	Outlining of moraine ridges as polygons. Break-in-slope between the moraine ridge and the surrounding terrain can be used as demarcation criterion (commonly visible in hillshaded DEMs).	Hubbard & Glasser (2005); Heyman et al. (2008); Blomdin et al. (2016a)
Glacial lineation	Elongated, streamlined sedimentary ridges, often occurring in clusters (swarms).	Several meters to hundreds of metres in width and length, several metres high	May be confused with non-glacial or bedrock structures.	Indicative of ice flow direction under warm-based conditions.	Identification from hillshades and slope DEMs. Mapping as lines along their centre lines and/or as polygons where they show distinctive asymmetric shapes and resolution of topographic data allows.	Kleman (1994); Blomdin et al. (2016a)
Scoured terrain	Undulating terrain, streamlined bedrock features and -basins, often paired with the occurrence of lakes	Areas of scoured terrain cover several km ²	Structures might reflect differences in resistance of different bedrock types to erosion; features might be concealed by sediments	Indicative of ice sheet- or ice cap- style glaciation; basal thermal regime at pressure-melting-point	Outlining of scoured terrain areas based on hillshades and slope DEMs to identify streamlined bedrock features and the absence of dendritic river patterns. Additional use of Google Earth imagery is recommended to identify lakes.	(Sugden, 1978; Sugden & John 1976)
Fluvial terrace	Smooth surfaces slightly inclined towards valley centre and in (paleo)flow direction. Consisting of either sediments or bedrock. Upslope and downslope limited by steep slopes.	Tens of square metres to several square kilometres	May be confused with structural benches, i.e. horizontal resistant bedrock units. Sometimes difficult to distinguish from very flat deposits of non-fluvial origin (e.g. mass movement deposits)	Remains of former fluvial valley bottoms. Indicative of climatic changes and / or base level changes.	Delineation of flat surfaces can be performed using a classified slope DEM. As demarcation criterion, the average slope of terrace surfaces identified based on field observations can be used as threshold value (< 4° in this study). unless distinguishable lobate patterns indicate the presence of alluvial or mass movement deposits	Stokes, Cunha, and Martins (2012); Bierman & Montgomery (2014)

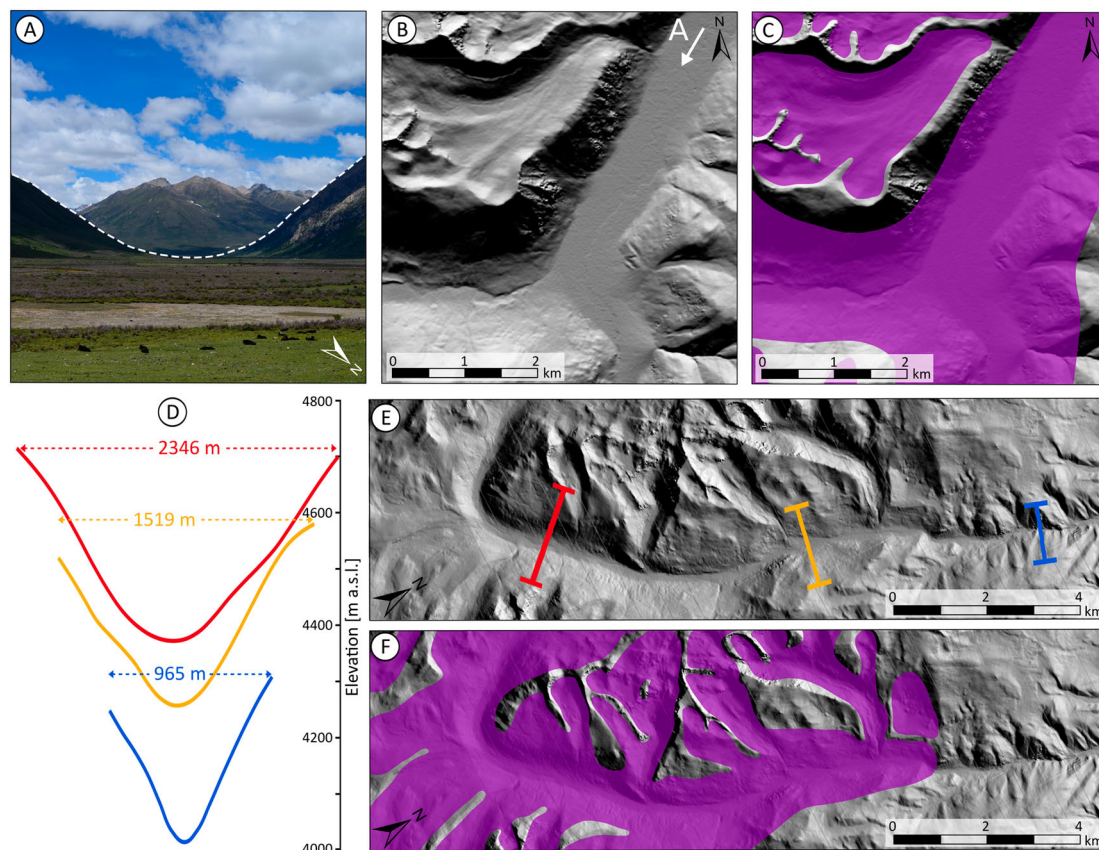


Figure 3. Example of mapped glacial valleys, as shown in (A) a field photograph, (B) a TanDEM-X hillshade (white arrow indicates photograph position and viewing direction), and (C) as represented on the geomorphological map. (D) Cross-valley profiles illustrating the down-valley progression from a parabolic glacial (red, orange) to a V-shaped fluvial valley (blue). (E) TanDEM-X hillshade with locations of the cross-profiles illustrated in (D). (F) Glacial valley extent in the geomorphological map based on valley profiles shown in (D) and (E). See Figure 2 for locations. TanDEM-X topographic data © DLR 2019.

glacial valleys have segments that start with steep, arcuate-shaped headwalls and gently sloping, glacially-eroded valley floors (cirques), and these are included in this category. Because fluvial valleys are commonly V-shaped and narrow, they are quite distinct from glacial valleys even though uncertainty in either identification can arise for valleys with a tectonic origin or where glacial valleys have a postglacial fluvial overprint (Stroeven et al., 2009).

Mapping of glacial valleys was based on identification criteria in Table 1, and features were outlined as polygons. Headwater valley outlines were identified from TanDEM-X-derived slope rasters and hillshades. The ArcGIS-profiling tool was employed to visually determine transitions in valley profiles, from upstream parabolic to downstream V-shaped.

Ice-marginal moraines are ridges that are mostly composed of unsorted debris deposited along the terminus of a glacier (Figure 4(A)). No subdivision into different moraine types has been pursued for the purpose of this study because all mapped ice-marginal features delineate former maximum ice extents (cf. Benn & Evans, 2013). Most moraines are indicative of warm-based glaciation (erosion of its substrate by sliding ice) because they typically contain subglacially transported sediment (Bierman & Montgomery,

2014). The outline and slope of ice-marginal moraines can be used to reconstruct the spatial extent and thickness of the depositing glaciers. The timing of deposition can often be construed from concentrations of cosmogenic nuclides in boulders residing on moraine crests (e.g. Chevalier & Replumaz, 2019; Fu et al., 2013b; Heyman et al., 2011b; Owen & Dortch, 2014). Uncertainty in the delineation of a moraine can arise if its size is small compared to the spatial resolution of the TanDEM-X satellite data, if the debris cover is thin or fragmented, or if the moraine is highly degraded (Blomdin et al., 2016a).

Ice-marginal moraines were mapped by outlining the ridges as polygons. The break-in-slope between the moraine ridge and the surrounding terrain, which is consistently visible in the hillshaded DEMs, was employed as a demarcation criterion.

Glacial lineations are elongated, streamlined ridges formed parallel to ice flow (Figure 4(B)). They form through subglacial deposition of till or erosion of bedrock and can typically be found in glacial valleys (Benn & Evans, 2013). Erosional glacial lineations consist of streamlined bedrock, while their depositional equivalents consist either solely of sediment, or have a bedrock core and sediment tail (e.g. crag-and-tails). No subdivision into different lineation types has been

pursued for the purpose of this study because all lineation types indicate the direction of warm-based ice flow. Confusion with non-glacial bedrock lineaments or tectonic structures may lead to identification errors (Blomdin et al., 2016a).

Glacial lineations were identified from hillshades and slope DEMs and mapped as lines along their centrelines. They were also delineated as polygons where they showed distinctive asymmetric shapes (Supplementary Material 1).

Scoured terrain is an undulating, low-relief bedrock surface of a knock-and-lochan type, typically with lakes in depressions and streamlined bedrock highs (glacial lineations), with a deranged river drainage pattern (Figure 4(B)). The scoured terrain is a result of areal erosion through glacial plucking and abrasion; processes which also require basal ice at the pressure melting point (Sugden & John, 1976).

Scoured terrain was mapped based on hillshades and slope DEMs to identify streamlined bedrock features and the absence of consistent river drainage patterns. In addition, the use of Google Earth imagery facilitated the identification of lakes as features typical of scoured terrain.

Fluvial terraces are characterised by even surfaces that gently slope towards the valley centre and in a downstream direction (Figure 5). These terraces terminate in steep slopes roughly parallel to the valley centre and may form staircase sequences (Stokes et al., 2012). Even though terraces can often be confidently identified from topographic data, it is equally often impossible to distinguish between strath terraces (which are eroded into bedrock) and alluvial terraces (consisting of incised floodplain deposits) without additional field verification. During field inspection (Figure 2) we sometimes identified bedrock outcrops, but, in all cases, those were found near the base of the lowest terrace slope. The terraces in our study area were therefore classified as alluvial terraces. Furthermore, they are defined as ‘fluvially incised’, because we cannot differentiate between different types of alluvial deposits at the scale of this map, which is largely based on remote sensing imagery.

In contrast to the straightforward strategy for the mapping of glacial landforms, the identification of terrace surfaces from hillshades and Google Earth imagery can be difficult. Especially in large tectonic basins, the differentiation between terrace surfaces and gently sloping alluvial or colluvial deposits poses

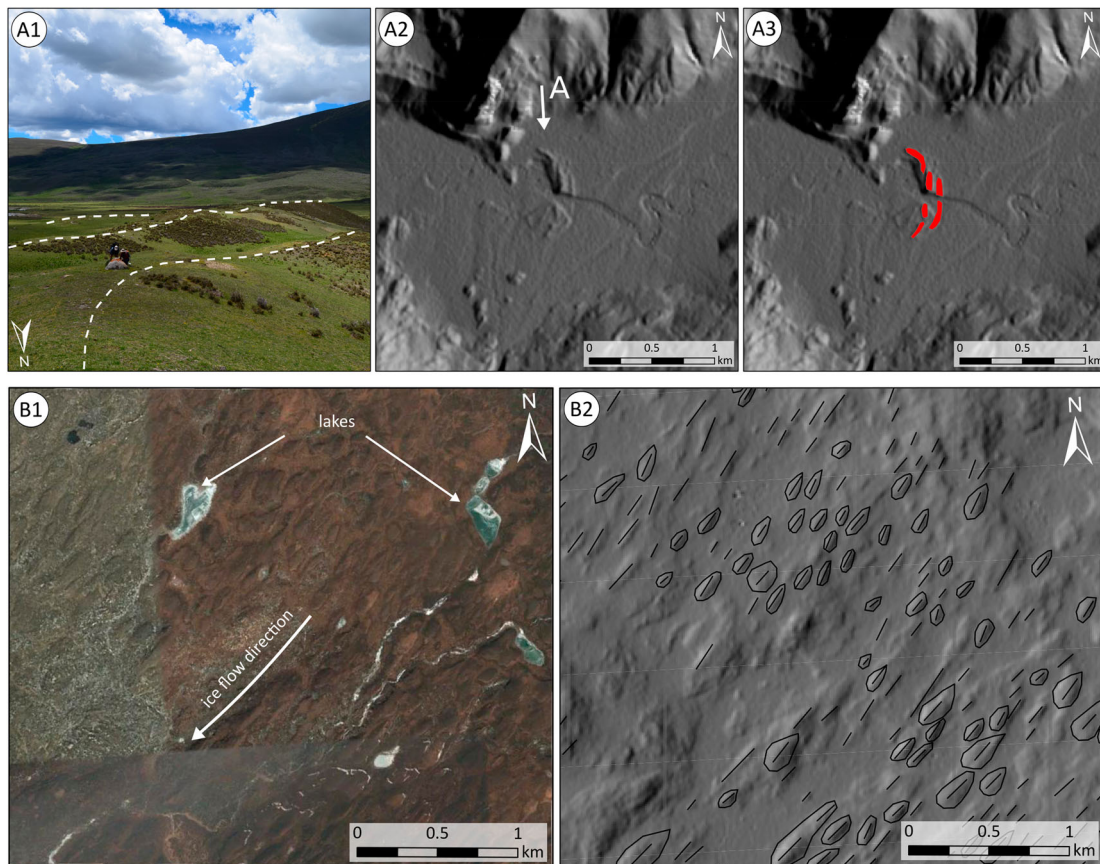


Figure 4. (A) Example of mapped ice-marginal moraines, as shown in (A1) a field photograph, (A2) a TanDEM-X hillshade (white arrow indicates photograph position and viewing direction), and (A3) as represented on the geomorphological map. (B) Example of a swarm of glacial lineations and scoured terrain on the Haizishan Plateau as expressed in (B1) a Google Earth image. White arrow shows ice flow direction. (B2) Glacial lineations mapped as lines on a TanDEM-X hillshade. Asymmetric features were additionally mapped as polygons. See Figure 2 for locations. TanDEM-X topographic data © DLR 2019.

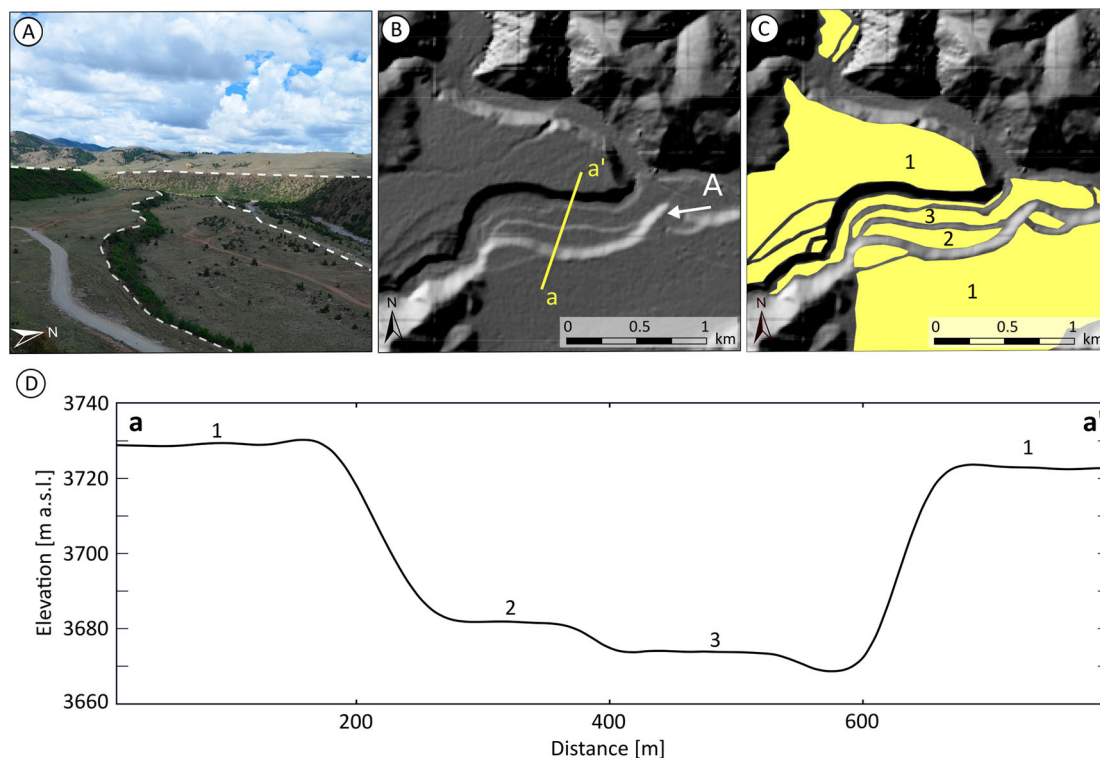


Figure 5. Examples of mapped fluvial terraces, as shown in (A) a field photograph, (B) a TanDEM-X hillshade, and (C) as represented on the geomorphological map. White arrow in (B) shows the photograph position and viewing direction and yellow line a-a' details the position of the profile in (D). (D) Cross-valley profile illustrating terrace morphology. Terrace numbering as in panel (C). See Figure 2 for location. TanDEM-X topographic data © DLR 2019.

a challenge. To reliably distinguish these landform types, the average slope of all terrace surfaces identified and mapped based on field observations were calculated and taken as the threshold value to create a classified slope model. Supported by field verification observations, surface inclinations below 4° were deemed indicative of fluvial terraces. The same threshold value was applied to areas outside of the field verification area unless distinguishable lobate patterns indicated the presence of alluvial or mass movement deposits.

3.3. Delineation of past ice extents

Based on the distribution of glacial landforms, we reconstruct a minimum extent of maximum glaciation (Figure 6; cf. Heyman et al., 2009; Blomdin et al., 2016a). It cannot be assumed that ice caps and glaciers within this area advanced to their maximum positions synchronously. Indeed, Fu et al. (2013a) show that the region experienced multiple cycles of glaciation. The chronological record for the wider region remains sparse (Chevalier et al., 2016; Chevalier & Replumaz, 2019; Fu et al., 2013b; Schäfer et al., 2002).

4. Results and discussion

Due to the high resolution of 12 m TanDEM-X, mapping was performed at an unprecedented level of detail.

Differences in resolution between TanDEM-X and digital elevation models used for previous mapping on the Tibetan Plateau (SRTM-90, SRTM-30) are clear from both a visual comparison (Figure 7), and from quantitative comparisons between our mapping results and a previous study by Fu et al. (2012) (Figure 8).

Evidence for paleoglaciation occurs primarily on plateaus and in mountains, with most extensive ice having built ice-marginal moraine complexes beyond valley confines. To document the extent of former glaciation, we mapped its four most common landforms; glacial valleys, glacial lineations, ice-marginal moraines, and scoured terrain. Glacial valleys cover 4080 km^2 , or 37% of the mapped area, and showcase the importance of deep glacial erosion during repeated glaciation. These valleys are common landscape elements of most mountains (as, for example, the Ge'Nyen massif in our study area) and ornament the margins of the Haizishan Plateau. Indeed, in the latter case, these glacial valleys are trunk valleys that lack alpine-style glaciation accumulation areas, and they signify the imprint of outlet glaciers from an ice cap that repeatedly covered the Haizishan Plateau (Fu et al., 2013a). In our study area, most glacial valleys span several kilometres in length and width. In contrast, valleys draining the lowest-elevation mountains ($< 4000 \text{ m a.s.l.}$) show no signs of glaciation.

Swarms of glacial lineations and scoured terrain are prominent on the Haizishan Plateau. Glacial

lineations are also present in some of the glacial valleys. The asymmetric shapes of some can be used to determine ice flow direction. The presence of scoured terrain, covering 354 km² of the mapped area, indicates the presence of ice-cap-style glaciation and supports the presence of warm-based ice as inferred by Fu et al. (2012, 2013a). On the very northern Haizishan Plateau, glacial lineations are difficult to distinguish from bedrock structures and fracturing, and so appear absent on the map (we were unable to access this area during fieldwork, see Figure 2 for the field verification route). The bulk of the 1310 glacial lineations mapped, ranging in length from 29 to 1335 m (Figure 8(A)), are from the Haizishan Plateau. Where they have distinct asymmetric (streamlined) shapes, they are indicative of ice flow direction (Supplementary Material 1). For example, they indicate ice flow outwards from a central ice dome towards the margins of the plateau, which is in accordance with paleoglaciological reconstructions by Fu et al. (2012, 2013a, 2013b). Furthermore, a funnelling of ice flow into glacial trunk valleys incised in the margins of the plateau can be reconstructed based on a spatial pattern of convergence of glacial lineations.

In total, 1237 individual ice-marginal moraine ridges were mapped, ranging from 2254 m² to over 2 km² (Figure 8(B)). They are primarily located along glacial valleys (where they appear as straight or arcuate ridges, or complexes of ridges) and at or beyond their mouths in tectonic basins, which are otherwise largely free of glacial landforms. Fu et al. (2012) found no evidence for ice-marginal moraines on the northern sector of the Haizishan Plateau, in the area considered in this study. We can largely confirm that absence (and thus its contrast with the southern half of the plateau) even though the increased resolution offered by TanDEM-X has allowed us to outline a small number of recessional moraines.

In addition to glacial landforms, 910 individual terrace surfaces were identified which are primarily located in four tectonic basins (i.e. Maoyaba, Litang, Kangga, Cuopo; Figure 2). Terraces appear as flat (< 4° inclination) surfaces in tectonic basins or river valleys with steep edges towards rivers. Their extents range from 1328 m² to 24.4 km² and amount to a surface area of approximately 265 km². Hence, terraces comprise around 2.4% of the mapped area. The

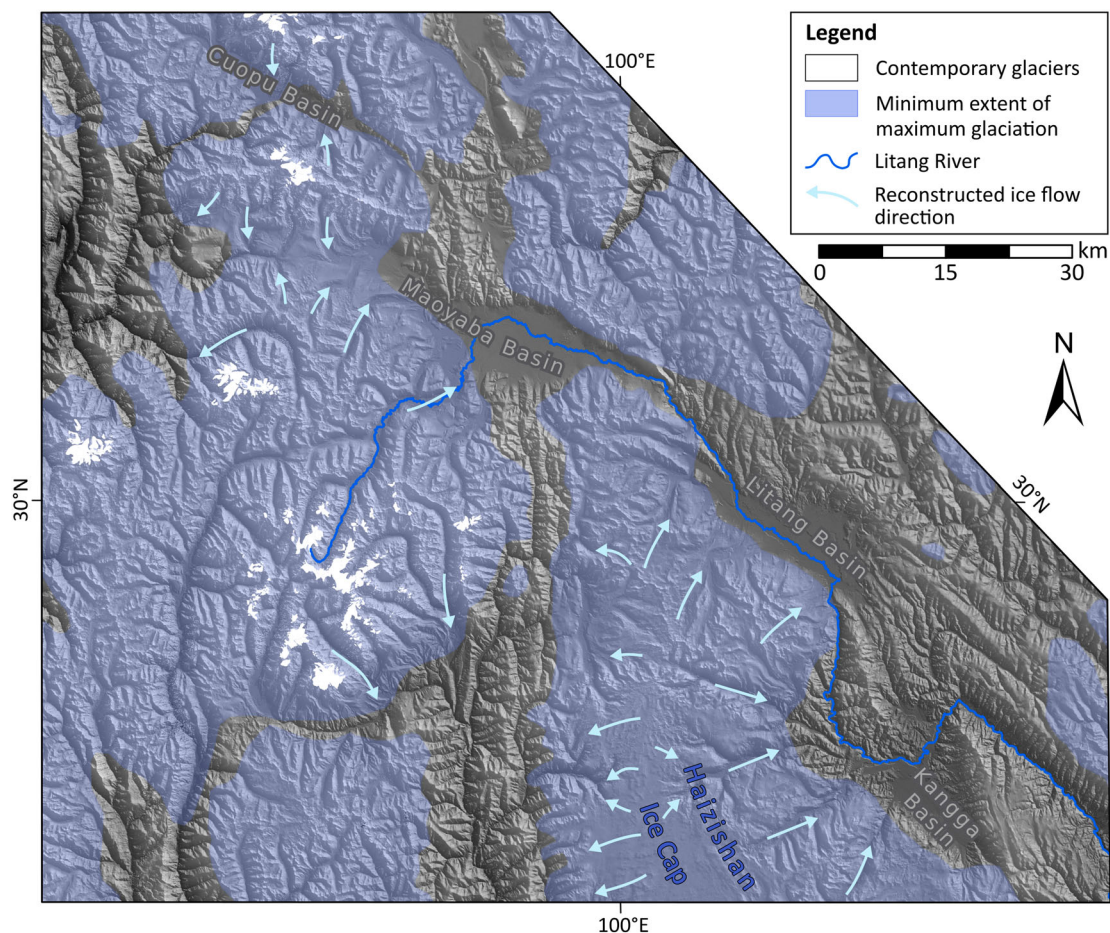


Figure 6. Minimum extent of maximum glacialiation in the study area (65% of mapped area), compared with present-day glacialiation (1% of mapped area). Light-blue arrows indicate reconstructed ice-flow directions from lineations. TanDEM-X topographic data © DLR 2019. A map showing the inferred minimum extent of maximum glacialiation which comprises 65% of the mapping area of this study. Contemporary glacialiation is also shown; it comprises an area of 1% of the mapping area. This map also shows the locations of the landforms presented in Figures 2–5.

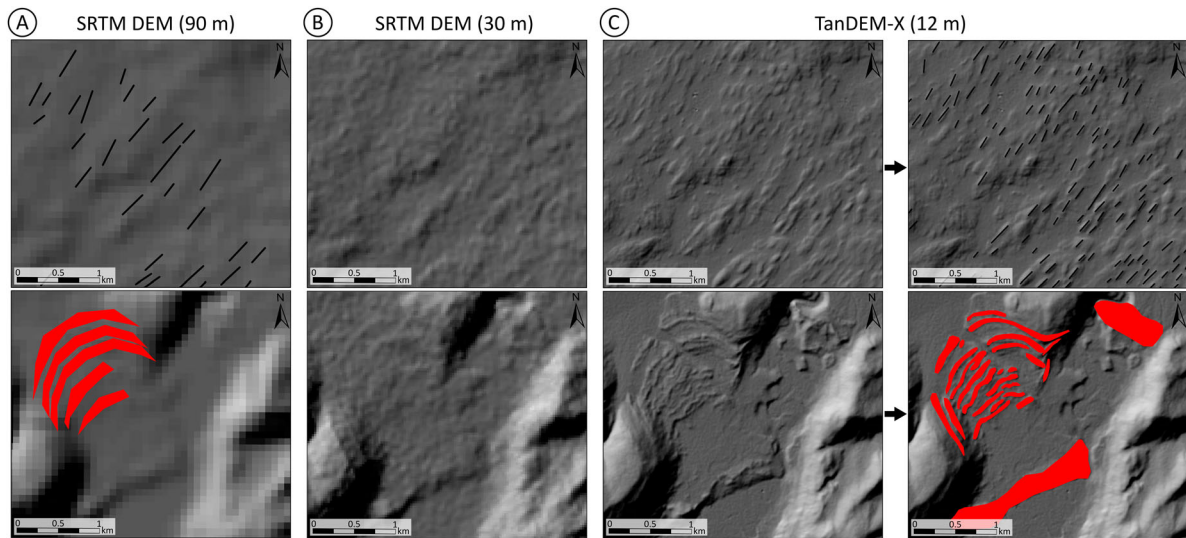


Figure 7. Different spatial resolutions of hillshades derived from different DEM products: (A) SRTM-90 and geomorphological mapping of Fu et al. (2012), (B) SRTM-30, and (C) TanDEM-X-12 (© DLR 2019). Upper row shows the same swarm of glacial lineations as in Figure 4(B), but at different resolution, and as represented in the geomorphological mapping of this study. Bottom row illustrates a similar comparison for ice-marginal moraines. See Figure 2 for locations.

presence of extensive terraces in tectonic basins indicates that these basins act as local sinks in the sediment budget, storing sediment emanating from upstream catchments.

The Haizishan Ice Cap and surrounding mountain glaciers have at times advanced across 65% of the mapped area judged from the distribution of glacial landforms (7101 km², Figure 6). We consider this footprint to represent the minimum extent of maximum glaciation because it is plausible that landforms associated with even further ice extents are either too small (e.g. degraded), buried underneath fluvial sediments, or only represented in the sedimentary record

(till, glaciofluvial deposits) or by scattered erratics (Heyman et al., 2009). To put these numbers in perspective, the paleoglaciological footprint of the Haizishan Ice Cap has been estimated to 3600 and 4000 km² (Fu et al., 2013a; Li et al., 1996), which is just over half the area of the contemporary Vatnajökull Ice Cap in Iceland. Ice expansion towards these limits of maximum glaciation was likely asynchronous across the mapped area, as evidenced by cosmogenic nuclide dating (Chevalier & Replumaz, 2019; Fu et al., 2013b).

The distribution of landforms presented in this study and the reconstructed glacial footprint quite

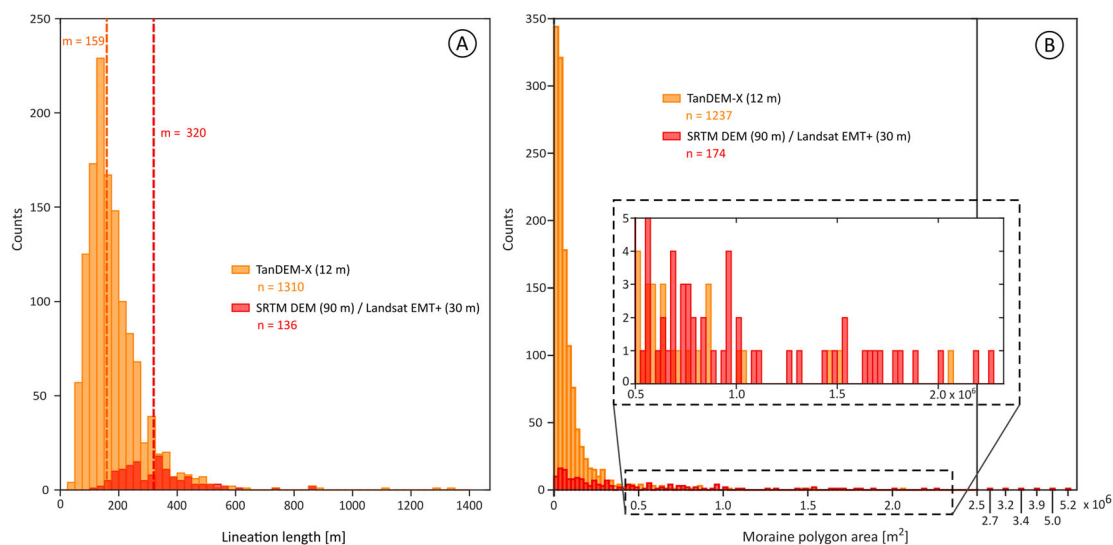


Figure 8. Histograms comparing mapping detail in this study (orange) with Fu et al. (2012) (red). (A) Counts and length of glacial lineations (bin width 25 m). (B) Counts and surface area of ice-marginal moraine polygons (bin width 0.025 km²). The higher spatial resolution of the data used for this study is reflected in the total number of mapped landforms (y-axes), in the median value (m) for glacial lineations, which is smaller for this study (159 m) compared to Fu et al. (2012) (320 m), and the higher number of smaller moraine polygons in this study.

consistently match the mapping by Fu et al. (2012). This congruence between the two independent mapping studies strengthens the presented reconstruction of the maximum paleo ice extent and indicates that a mapping approach based on SRTM and Landsat data remains suitable for reconstructing regional Tibetan paleoglaciology. This new study adds more and smaller landforms and therefore important detail to established patterns (Figures 7 and 8). For example, because Fu et al. (2012) were limited to landforms larger than 70 m due to the spatial resolution of their data, the minimum length among the 136 glacial lineations in their study is 109 m, compared to 29 m in this study. The possibility to identify a larger range of lineation lengths and more lineations makes reconstructions of ice flow directions more robust, especially in places where streamlined shapes can be distinguished (Figure 4(B)).

When only the area of overlap between the two studies is considered, Fu et al. (2012) found that the smallest out of their 174 mapped individual moraines had a size of 13,011 m², which is more than five times larger than the smallest moraine mapped here (2254 m²). On the contrary, their largest moraine of almost 5.2 km² (Figure 8(B)) is more than twice the size of the largest moraine in this study (almost 2.1 km²). The 12 m TanDEM-X largest moraine is significantly smaller because individual ridges were differentiated in instances where the previous study aggregated these into complexes of several moraines. This differentiation attests again to the level of detail afforded by 12 m TanDEM-X.

The fluvial terraces mapped in this study provide an addition to the glacial landform record by adding information about the distribution of a prominent class of primarily fluvial features. Their correct identification has been confirmed through field verification in the Kangga and Maoyaba Basins (Figure 2). Moreover, the dating of these terraces allows for a bracketing of moraine ages with independent ages of upstream and downstream terraces in geochronological studies.

The reconstructed glaciation footprint supports a prevalence for ice cap- and alpine styles of glaciation on the SE Tibetan Plateau. In comparison with previous studies, the level of detail achieved using 12 m TanDEM-X illustrates the potential for increasingly detailed reconstructions of ice dynamics and ice margin locations. The presence of fluvial terraces in direct conjunction with traces of glaciation (end moraines, glacial valleys), may imply a modification of the glacial landscape by fluvial processes (removal or burial of moraines). The novel approach of this study, to map fluvial terraces in addition to glacial landforms, allows for testing the temporal relationship between glaciation and fluvial deposition and, if coupled, to increase the precision in the timing of glaciations.

5. Summary

We present a map of the distribution of glacial valleys, ice-marginal moraines, glacial lineations, and scoured terrain, using 12 m TanDEM-X digital elevation data, to provide an alternative estimate on the former extents of ice caps and valley glaciers in the Shaluli Shan, south-eastern Tibetan Plateau, an area previously mapped by us using lower-resolution satellite data. As an additional approach, novel for this region, we mapped fluvial terraces. The overall distribution of landforms is objectively highly similar to the previous product and also the paleoglaciological footprint of glaciation (i.e. the minimum extent of maximum glaciation) is consistent with previous mapping. Although we have mapped many more and smaller landforms, this similarity indicates that a mapping approach based on SRTM and Landsat data remains suitable for reconstructing regional Tibetan paleoglaciology. Landform distribution indicates a prevalence of ice cap- and alpine styles of glaciation. The higher mapping resolution of our study and the addition of fluvial terraces provides a basis for detailed geomorphological and geochronological studies of these glaciation patterns and highlights the potential of high-resolution 12 m TanDEM-X for the identification of glacial and fluvial geomorphology and the benefits of such data for landscape evolution studies.

Software

Data processing, analysis and landform mapping was conducted in ArcMap 10.7.1. The final map layout was created in Inkscape version 0.92.3.

Data

ESRI shapefiles used in the production of the map are provided as supplementary material.

Acknowledgements

The authors thank the German Aerospace Center (DLR) for the provision of the 12 m TanDEM-X data (project identifier: DEM_GEOL2742).

Disclosure statement

No potential conflict of interest was reported by the author(s).

Funding

Funding for complementary fieldwork in June 2019 was supported by the Institute of Tibetan Plateau Research, Chinese Academy of Sciences, Beijing (Strategic Priority Research Program of Chinese Academy of Sciences, grant number XDA20100300), the Geomorphology and Glaciology research unit at the Department of Physical Geography,

Stockholm University, and a stipend from the Albert and Maria Bergström foundation to Ramona Schneider.

ORCID

R.A.A. Schneider  <http://orcid.org/0000-0003-1577-7587>
 R. Blomdin  <http://orcid.org/0000-0003-0306-5291>
 P. Fu  <http://orcid.org/0000-0002-3759-9403>
 X.K. Xu  <http://orcid.org/0000-0002-5410-015X>
 A.P. Stroeven  <http://orcid.org/0000-0001-8812-2253>

References

- Barr, I. D., & Lovell, H. (2014). A review of topographic controls on moraine distribution. *Geomorphology*, 226, 44–64. <https://doi.org/10.1016/j.geomorph.2014.07.030>
- Benn, D. I., & Evans, D. J. A. (2013). *Glaciers & glaciation* (2nd ed). Routledge.
- Bierman, P. R., & Montgomery, D. R. (2014). *Key concepts in geomorphology*. W.H. Freeman and Company Publishers: A Macmillan Higher Education Company.
- Blomdin, R., Heyman, J., Stroeven, A. P., Hättestrand, C., Harbor, J. M., Gribenski, N., Jansson, K. N., Petrakov, D. A., Ivanov, M. N., Alexander, O., Rudoy, A. N., & Walther, M. (2016a). Glacial geomorphology of the Altai and Western Sayan Mountains, Central Asia. *Journal of Maps*, 12(1), 123–136. <https://doi.org/10.1080/17445647.2014.992177>
- Blomdin, R., Stroeven, A. P., Harbor, J. M., Gribenski, N., Caffee, M. W., Heyman, J., Rogozhina, I., Ivanov, M. N., Petrakov, D. A., Walther, M., Rudoy, A. N., Zhang, W., Orkhonselenge, A., Hättestrand, C., Lifton, N. A., & Jansson, K. N. (2018). Timing and dynamics of glaciation in the Ikh Turgen Mountains, Altai region, high Asia. *Quaternary Geochronology*, 47, 54–71. <https://doi.org/10.1016/j.quageo.2018.05.008>
- Blomdin, R., Stroeven, A. P., Harbor, J. M., Lifton, N. A., Heyman, J., Gribenski, N., Petrakov, D. A., Caffee, M. W., Ivanov, M. N., Hättestrand, C., Rogozhina, I., & Usabaliev, R. (2016b). Evaluating the timing of former glacier expansions in the Tian Shan: A key step towards robust spatial correlations. *Quaternary Science Reviews*, 153, 78–96. <https://doi.org/10.1016/j.quascirev.2016.07.029>
- Boulton, S. J., & Stokes, M. (2018). Which DEM is best for analyzing fluvial landscape development in mountainous terrains? *Geomorphology*, 310, 168–187. <https://doi.org/10.1016/j.geomorph.2018.03.002>
- Bridgland, D., & Westaway, R. (2008). Climatically controlled river terrace staircases: A worldwide Quaternary phenomenon. *Geomorphology*, 98(3–4), 285–315. <https://doi.org/10.1016/j.geomorph.2006.12.032>
- Chandler, B. M. P., Lovell, H., Boston, C. M., Lukas, S., Barr, I. D., Benediktsson, I. O., Benn, D. I., Clark, C. D., Darvill, C. M., Evans, D. J. A., Ewertowski, M. W., Loibl, D., Margold, M., Otto, J.-C., Roberts, D. H., Stokes, C. R., Storrar, R. D., & Stroeven, A. P. (2018). Glacial geomorphological mapping: A review of approaches and frameworks for best practice. *Earth-Science Reviews*, 185, 806–846. <https://doi.org/10.1016/j.earscirev.2018.07.015>
- Charrier, R., & Li, Y. (2012). Assessing resolution and source effects of digital elevation models on automated floodplain delineation: A case study from the Camp Creek Watershed, Missouri. *Applied Geography*, 34, 38–46. <https://doi.org/10.1016/j.apgeog.2011.10.012>
- Chen, R., Zhou, S., Li, Y., & Deng, Y. (2016). Glacial geomorphology of the Parlung Zangbo Valley, southeastern Tibetan Plateau. *Journal of Maps*, 12(5), 716–724. <https://doi.org/10.1080/17445647.2015.1069765>
- Chevalier, M.-L., Leloup, P. H., Replumaz, A., Pan, J., Liu, D., Li, H., Gournbet, L., & Métois, M. (2016). Tectonic-geomorphology of the Litang fault system, SE Tibetan Plateau, and implication for regional seismic hazard. *Tectonophysics*, 682, 278–292. <https://doi.org/10.1016/j.tecto.2016.05.039>
- Chevalier, M.-L., & Replumaz, A. (2019). Deciphering old moraine age distributions in SE Tibet showing bimodal climatic signal for glaciations: Marine Isotope Stages 2 and 6. *Earth and Planetary Science Letters*, 507, 105–118. <https://doi.org/10.1016/j.epsl.2018.11.033>
- Clark, M. K., House, M. A., Royden, L. H., Whipple, K. X., Burchfiel, B. C., Zhang, X., & Tang, W. (2005). Late Cenozoic uplift of southeastern Tibet. *Geology*, 33(6), 525. <https://doi.org/10.1130/G21265.1>
- Cordier, S., Adamson, K., Delmas, M., Calvet, M., & Harmand, D. (2017). Of ice and water: Quaternary fluvial response to glacial forcing. *Quaternary Science Reviews*, 166, 57–73. <https://doi.org/10.1016/j.quascirev.2017.02.006>
- Dortch, J. M., Owen, L. A., & Caffee, M. W. (2013). Timing and climatic drivers for glaciation across semi-arid western Himalayan–Tibetan orogen. *Quaternary Science Reviews*, 78, 188–208. <https://doi.org/10.1016/j.quascirev.2013.07.025>
- Farinotti, D., Immerzeel, W. W., de Kok, R. J., Quincey, D. J., & Dehecq, A. (2020). Manifestations and mechanisms of the Karakoram glacier Anomaly. *Nature Geoscience*, 13(1), 8–16. <https://doi.org/10.1038/s41561-019-0513-5>
- Fielding, E., Isacks, B., Barazangi, M., & Duncan, C. (1994). How flat is Tibet? *Geology*, 22(2), 163–167. [https://doi.org/10.1130/0091-7613\(1994\)022<0163:HFIT>2.3.CO;2](https://doi.org/10.1130/0091-7613(1994)022<0163:HFIT>2.3.CO;2)
- Fu, P., Harbor, J. M., Stroeven, A. P., Hättestrand, C., Heyman, J., & Zhou, L. (2013a). Glacial geomorphology and paleoglaciation patterns in Shaluli Shan, the southeastern Tibetan Plateau – evidence for polythermal ice cap glaciation. *Geomorphology*, 182, 66–78. <https://doi.org/10.1016/j.geomorph.2012.10.030>
- Fu, P., Heyman, J., Hättestrand, C., Stroeven, A. P., & Harbor, J. M. (2012). Glacial geomorphology of the Shaluli Shan area, southeastern Tibetan Plateau. *Journal of Maps*, 8(1), 48–55. <https://doi.org/10.1080/17445647.2012.668762>
- Fu, P., Stroeven, A. P., Harbor, J. M., Hättestrand, C., Heyman, J., Caffee, M. W., & Zhou, L. (2013b). Paleoglaciation of Shaluli Shan, southeastern Tibetan Plateau. *Quaternary Science Reviews*, 64, 121–135. <https://doi.org/10.1016/j.quascirev.2012.12.009>
- Fu, P., Stroeven, A. P., Harbor, J. M., Heyman, J., Hättestrand, C., & Caffee, M. W. (2019). Ice cap erosion patterns from bedrock ¹⁰Be and ²⁶Al, southeastern Tibetan Plateau. *Earth Surface Processes and Landforms*, 44(4), 918–932. <https://doi.org/10.1002/esp.4544>
- Glasser, N. F., & Bennett, M. R. (2004). Glacial erosional landforms: Origins and significance for palaeogeology. *Progress in Physical Geography: Earth and Environment*, 28(1), 43–75. <https://doi.org/10.1191/0309133304p401ra>
- GLIMS, NSIDC. (2018). *Global Land Ice Measurements from space glacier database*. Compiled and made available by the international GLIMS community and the National Snow and Ice Data Center, Boulder CO, U.S.A. doi:10.7265/N5V98602.

- Gribenski, N., Jansson, K. N., Preusser, F., Harbor, J. M., Stroeven, A. P., Trauerstein, M., Blomdin, R., Heyman, J., Caffee, M. W., Lifton, N. A., & Zhang, W. (2018). Re-evaluation of MIS 3 glaciation using cosmogenic radionuclide and single grain luminescence ages, Kanas Valley, Chinese Altai. *Journal of Quaternary Science*, 33(1), 55–67. <https://doi.org/10.1002/jqs.2998>
- Grohmann, C. H. (2018). Evaluation of TanDEM-X DEMs on selected Brazilian sites: Comparison with SRTM, ASTER GDEM and ALOS AW3D30. *Remote Sensing of Environment*, 212, 121–133. <https://doi.org/10.1016/j.rse.2018.04.043>
- Hewitt, K. (2005). The Karakoram Anomaly? Glacier expansion and the ‘Elevation Effect,’ Karakoram Himalaya. *Mountain Research and Development*, 25(4), 332–340. [https://doi.org/10.1659/0276-4741\(2005\)025\[0332:TKAGEA\]2.0.CO;2](https://doi.org/10.1659/0276-4741(2005)025[0332:TKAGEA]2.0.CO;2)
- Heyman, J., Hättestrand, C., & Stroeven, A. P. (2008). Glacial geomorphology of the Bayan Har sector of the NE Tibetan Plateau. *Journal of Maps*, 4(1), 42–62. <https://doi.org/10.4113/jom.2008.96>
- Heyman, J., Stroeven, A. P., Alexanderson, H., Hättestrand, C., Harbor, J., Li, Y. K., Caffee, M. W., Zhou, L. P., Veres, D., Liu, F., & Machiedo, M. (2009). Palaeoglaciology of Bayan Har Shan, northeastern Tibetan Plateau: Glacial geology indicates maximum extents limited to ice cap and ice field scales. *Journal of Quaternary Science*, 24(7), 710–727. <https://doi.org/10.1002/jqs.1305>
- Heyman, J., Stroeven, A. P., Caffee, M. W., Hättestrand, C., Harbor, J. M., Li, Y. K., Alexanderson, H., Zhou, L. P., & Hubbard, A. (2011a). Palaeoglaciology of Bayan Har Shan, NE Tibetan Plateau: Exposure ages reveal a missing LGM expansion. *Quaternary Science Reviews*, 30(15–16), 1988–2001. <https://doi.org/10.1016/j.quascirev.2011.05.002>
- Heyman, J., Stroeven, A. P., Harbor, J. M., & Caffee, M. W. (2011b). Too young or too old: Evaluating cosmogenic exposure dating based on an analysis of compiled boulder exposure ages. *Earth and Planetary Science Letters*, 302(1–2), 71–80. <https://doi.org/10.1016/j.epsl.2010.11.040>
- Hubbard, B., & Glasser, N. F. (2005). *Field techniques in glaciology and glacial geomorphology*. Wiley.
- Kassab, C., Wang, J., & Harbor, J. (2013). Glacial geomorphology of the Dalijia Shan region, northeastern Tibetan Plateau. *Journal of Maps*, 9(1), 98–105. <https://doi.org/10.1080/17445647.2012.754729>
- Kleman, J. (1994). Preservation of landforms under ice sheets and ice caps. *Geomorphology*, 9, 19–32.
- Lehmkuhl, F., & Owen, L. (2005). Late Quaternary glaciation of Tibet and the bordering mountains: A review. *Boreas*, 34(2), 87–100. <https://doi.org/10.1080/03009480510012908>
- Li, J. J., Feng, Z., & Zhou, S. Z. (1996). The Quaternary glacial remnants in Hengduan mountain. In J. J. Li & Z. Su (Eds.), *Glaciers in Hengduan Mountains* (pp. 157–212). Science Press.
- Li, Y. K., Harbor, J., Stroeven, A. P., Fabel, D., Kleman, J., Fink, D., Caffee, M., & Elmore, D. (2005). Ice sheet erosion patterns in valley systems in northern Sweden investigated using cosmogenic nuclides. *Earth Surface Processes and Landforms*, 30(8), 1039–1049. <https://doi.org/10.1002/esp.1261>
- Lindholm, M. S., & Heyman, J. (2016). Glacial geomorphology of the Maidika region, Tibetan Plateau. *Journal of Maps*, 12(5), 797–803. <https://doi.org/10.1080/17445647.2015.1078182>
- Liu, G., Li, X., Chiang, H.-W., Cheng, H., Yuan, S., Chawchai, S., He, S., Lu, Y., Aung, L. T., Maung, P. M., Tun, W. N., Oo, K. M., & Wang, X. (2020). On the glacial-interglacial variability of the Asian monsoon in speleothem $\delta^{18}\text{O}$ records. *Science Advances*, 6(7), eaay8189. <https://doi.org/10.1126/sciadv.aay8189>
- Maddy, D., Bridgland, D., & Westaway, R. (2001). Uplift-driven valley incision and climate-controlled river terrace development in the Thames Valley, UK. *Quaternary International*, 79(1), 23–36. [https://doi.org/10.1016/S1040-6182\(00\)00120-8](https://doi.org/10.1016/S1040-6182(00)00120-8)
- Minár, J., & Evans, I. S. (2008). Elementary forms for land surface segmentation: The theoretical basis of terrain analysis and geomorphological mapping. *Geomorphology*, 95(3–4), 236–259. <https://doi.org/10.1016/j.geomorph.2007.06.003>
- Molnar, P., & England, P. (1990). Late Cenozoic uplift of mountain ranges and global climate change: Chicken or egg? *Nature*, 346(6279), 29–34. <https://doi.org/10.1038/346029a0>
- Morén, B., Heyman, J., & Stroeven, A. P. (2011). Glacial geomorphology of the central Tibetan Plateau. *Journal of Maps*, 7(1), 115–125. <https://doi.org/10.4113/jom.2011.1161>
- Murari, M. K., Owen, L. A., Dortch, J. M., Caffee, M. W., Dietsch, C., Fuchs, M., Haneberg, W. C., Sharma, M. C., & Townsend-Small, A. (2014). Timing and climatic drivers for glaciation across monsoon-influenced regions of the Himalayan–Tibetan orogen. *Quaternary Science Reviews*, 88, 159–182. <https://doi.org/10.1016/j.quascirev.2014.01.013>
- Oerlemans, J., & Fortuin, J. P. F. (1992). Sensitivity of glaciers and small ice caps to greenhouse warming. *Science*, 258(5079), 115–117. <https://doi.org/10.1126/science.258.5079.115>
- Olszak, J. (2017). Climatically controlled terrace staircases in uplifting mountainous areas. *Global and Planetary Change*, 156, 13–23. <https://doi.org/10.1016/j.gloplacha.2017.07.013>
- Owen, L. A., & Dortch, J. M. (2014). Nature and timing of Quaternary glaciation in the Himalayan–Tibetan orogen. *Quaternary Science Reviews*, 88, 14–54. <https://doi.org/10.1016/j.quascirev.2013.11.016>
- Pánek, T., Schönfeldt, E., Winocur, D., Břežný, M., Šilhán, K., Chalupa, V., & Korup, O. (2020). moraines and marls: Giant landslides of the Lago Pueyrredón valley in Patagonia, Argentina. *Quaternary Science Reviews*, 248, 106598. <https://doi.org/10.1016/j.quascirev.2020.106598>
- Pasquetti, F., Bini, M., & Ciampalini, A. (2019). Accuracy of the TanDEM-X digital elevation model for coastal geomorphological studies in Patagonia (South Argentina). *Remote Sensing*, 11(15), 1767. <https://doi.org/10.3390/rs11151767>
- Pipaud, I., Loibl, D., & Lehmkuhl, F. (2015). Evaluation of TanDEM-X elevation data for geomorphological mapping and interpretation in high mountain environments — A case study from SE Tibet, China. *Geomorphology*, 246, 232–254. <https://doi.org/10.1016/j.geomorph.2015.06.025>
- Raymo, M. E., & Ruddiman, W. F. (1992). Tectonic forcing of late Cenozoic climate. *Nature*, 359(6391), 117–122. <https://doi.org/10.1038/359117a0>
- Schäfer, J. M., Tschudi, S., Zhao, Z., Wu, X., Ivy-Ochs, S., Wieler, R., Baur, H., Kubik, P. W., & Schlüchter, C. (2002). The limited influence of glaciations in Tibet on global climate over the past 170 000 yr. *Earth and*

- Planetary Science Letters*, 194(3–4), 287–297. [https://doi.org/10.1016/S0012-821X\(01\)00573-8](https://doi.org/10.1016/S0012-821X(01)00573-8)
- Schmidt, J., & Andrew, R. (2005). Multi-scale landform characterization. *Area*, 37(3), 341–350. <https://doi.org/10.1111/j.1475-4762.2005.00638.x>
- Shulmeister, J., Davies, T. R., Evans, D. J. A., Hyatt, O. M., & Tovar, D. S. (2009). Catastrophic landslides, glacier behaviour and moraine formation – A view from an active plate margin. *Quaternary Science Reviews*, 28, 1085–1096. <https://doi.org/10.1016/j.quascirev.2008.11.015>
- Starkel, L. (2003). Climatically controlled terraces in uplifting mountain areas. *Quaternary Science Reviews*, 22(20), 2189–2198. [https://doi.org/10.1016/S0277-3791\(03\)00148-3](https://doi.org/10.1016/S0277-3791(03)00148-3)
- Stokes, M., Cunha, P. P., & Martins, A. A. (2012). Techniques for analysing Late Cenozoic river terrace sequences. *Geomorphology*, 165–166, 1–6. <https://doi.org/10.1016/j.geomorph.2012.03.022>
- Stroeven, A. P., Hättestrand, C., Heyman, J., Harbor, J., Li, Y. K., Zhou, L. P., Caffee, M. W., Alexanderson, H., Kleman, J., Ma, H. Z., & Liu, G. N. (2009). Landscape analysis of the Huang He headwaters, NE Tibetan Plateau — patterns of glacial and fluvial erosion. *Geomorphology*, 103(2), 212–226. <https://doi.org/10.1016/j.geomorph.2008.04.024>
- Stroeven, A. P., Hättestrand, C., Heyman, J., Kleman, J., & Morén, B. M. (2013). Glacial geomorphology of the Tian Shan. *Journal of Maps*, 9(4), 505–512. <https://doi.org/10.1080/17445647.2013.820879>
- Sugden, D. E. (1978). Glacial erosion by the Laurentide Ice Sheet. *Journal of Glaciology*, 20(83), 367–391. <https://doi.org/10.3189/S002214300013915>
- Sugden, D. E., & John, B. S. (1976). *Glaciers and landscape: A geomorphological approach*. Edward Arnold.
- Viveen, W., Baby, P., Sanjurjo-Sanchez, J., & Hurtado-Enríquez, C. (2020). Fluvial terraces as quantitative markers of late Quaternary detachment folding and creeping thrust faulting in the Peruvian Huallaga basin. *Geomorphology*, 367, 107315. <https://doi.org/10.1016/j.geomorph.2020.107315>
- Wang, C., Zhao, X., Liu, Z., Lippert, P. C., Graham, S. A., Coe, R. S., Yi, H., Zhu, L., Liu, S., & Li, Y. (2008). Constraints on the early uplift history of the Tibetan plateau. *Proceedings of the National Academy of Sciences*, 105(13), 4987–4992. <https://doi.org/10.1073/pnas.0703595105>
- Wang, Y., Zheng, J., Zhang, W., Li, S., Liu, X., Yang, X., & Liu, Y. (2012). Cenozoic uplift of the Tibetan Plateau: Evidence from the tectonic–sedimentary evolution of the western Qaidam Basin. *Geoscience Frontiers*, 3(2), 175–187. <https://doi.org/10.1016/j.gsf.2011.11.005>
- Wessel, B. (2018). *TanDEM-X Ground Segment – DEM Products Specification Document*, EOC, DLR, Oberpfaffenhofen, Germany, Public Document TD-GS-PS-0021, Issue 3.2. [Online]. <https://tandemx-science.dlr.de/>. https://geoservice.dlr.de/web/dataguide/tdm90/pdfs/TD-GS-PS-0021_DEM-Product-Specification.pdf
- Xu, L., & Zhou, S. (2009). Quaternary glaciations recorded by glacial and fluvial landforms in the Shaluli mountains, southeastern Tibetan plateau. *Geomorphology*, 103(2), 268–275. <https://doi.org/10.1016/j.geomorph.2008.04.015>
- Xu, L., & Zhou, S. (2014). Late Quaternary fluvial terraces near the Daocheng Ice Cap, eastern Tibetan plateau. *Quaternary Research*, 81(3), 452–463. <https://doi.org/10.1016/j.yqres.2013.08.007>
- Yan, Q., Owen, L. A., Wang, H., & Zhang, Z. (2018). Climate constraints on glaciation over high-mountain Asia during the last glacial maximum. *Geophysical Research Letters*, 45, 9024–9033.
- Yan, Q., Owen, L. A., Zhang, Z., Jiang, N., & Zhang, R. (2020). Deciphering the evolution and forcing mechanisms of glaciation over the Himalayan-Tibetan orogen during the past 20,000 years. *Earth and Planetary Science Letters*, 541, 116295. <https://doi.org/10.1016/j.epsl.2020.116295>
- Yao, T., Duan, K., Thompson, L. G., Wang, N., Tian, L., Xu, B., Wang, Y., & Yu, W. (2007). Temperature variations over the past millennium on the Tibetan Plateau revealed by four ice cores. *Annals of Glaciology*, 46, 362–366. <https://doi.org/10.3189/172756407782871305>
- Yao, T., Masson-Delmotte, V., Gao, J., Yu, W., Yang, X., Risi, C., Sturm, C., Werner, M., Zhao, H., He, Y., Ren, W., Tian, L., Shi, C., & Hou, S. (2013). A review of climatic controls on $\delta^{18}\text{O}$ in precipitation over the Tibetan Plateau: Observations and simulations. *Reviews of Geophysics*, 51(4), 525–548. <https://doi.org/10.1002/rog.20023>
- Yao, T., Thompson, L. G., Mosbrugger, V., Zhang, F., Ma, Y., Luo, T., Xu, B., Yang, X., Joswiak, D. R., Wang, W., Joswiak, M. E., Devkota, L. P., Tayal, S., Jilani, R., & Fayziev, R. (2012b). Third pole Environment (TPE). *Environmental Development*, 3, 52–64. <https://doi.org/10.1016/j.envdev.2012.04.002>
- Yao, T., Thompson, L., Yang, W., Yu, W., Gao, Y., Guo, X., Yang, X., Duan, K., Zhao, H., Xu, B., Pu, J., Lu, A., Xiang, Y., Kattel, D. B., & Joswiak, D. (2012a). Different glacier status with atmospheric circulations in Tibetan Plateau and surroundings. *Nature Climate Change*, 2(9), 663–667. <https://doi.org/10.1038/nclimate1580>
- Zeng, Q., Zhang, L., Davies, T., Yuan, G., Xue, X., Wei, R., Yin, Q., & Liao, L. (2019). Morphology and inner structure of Luanshibao rock avalanche in Litang, China and its implications for long-runout mechanisms. *Engineering Geology*, 260, 105216. <https://doi.org/10.1016/j.enggeo.2019.105216>
- Zhang, R., Jiang, D., Ramstein, G., Zhang, Z., Lippert, P. C., & Yu, E. (2018). Changes in Tibetan Plateau latitude as an important factor for understanding east Asian climate since the Eocene: A modeling study. *Earth and Planetary Science Letters*, 484, 295–308. <https://doi.org/10.1016/j.epsl.2017.12.034>
- Zhang, Z., Wang, J., Xu, X., Bai, S., & Chang, Z. (2015). Cosmogenic ^{10}Be and ^{26}Al chronology of the last glaciation of the Palaeo-Daocheng Ice Cap, Southeastern Qinghai-Tibetan Plateau. *Acta Geologica Sinica - English Edition*, 89(2), 575–584. <https://doi.org/10.1111/1755-6724.12448>